Aerogel sponges of silk fibroin, hyaluronic acid and heparin for soft tissue engineering: Composition-properties relationship

Mathie NAJBERG[a,b], Muhammad HAJI MANSOR[b], Théodore TAILLÉ[b], Céline BOURÉ[b], Rodolfo MOLINA-PEÑA[b], Frank BOURY[b], José-Luis CENIS[c], Emmanuel GARCION[b#*] & Carmen ALVAREZ-LORENZO[a#*]

[a] Departamento de Farmacología, Farmacia y Tecnología Farmacéutica, I+DFarma (GI-1645), Facultad de Farmacia, Universidade de Santiago de Compostela, 15782-Santiago de Compostela, Spain

[b] CRCINA, INSERM, Université de Nantes, Université d'Angers, Angers, France

[c] Biotechnology Department, Instituto Murciano de Investigación y Desarrollo Agrario y Alimentario (IMIDA), 30150 La Alberca, Murcia, Spain.

[#]Equivalent contribution

* Corresponding authors:

E. Garcion, email: emmanuel.garcion@univ-angers.fr; Phone: +33 (0)244688543

C. Alvarez-Lorenzo, email: carmen.alvarez.lorenzo@usc.es; Phone: +34 881815239

ABSTRACT

This work aims to design biocompatible aerogel sponges that can host and control the release of stromal cell-derived factor-1α (SDF-1α or CXCL12), a key protein for applications ranging from regenerative medicine to cancer therapy (notably for neural tissues). Miscibility of silk fibroin (SF) and hyaluronic acid (HA) was investigated by means of fluorescence and scanning electron microscopy to identify processing conditions. Series of freeze-dried sponges were prepared by associating and cross-linking within the same 3D structure, HA, SF, poly-L-lysine (PLL) and heparin (hep). Aerogel sponges presented high swelling degree and porosity (~90%), adequate mean pore diameter (ca. 60 µm) and connectivity for welcoming cells, and a soft texture close to that of the brain (6-13 kPa Young's Modulus). Addition of SF yielded sponges with slower biodegradation. SF-HA and SF-HA-hep sponges retained 75% and 93% of the SDF-1α respectively after 7 days and were found to be cytocompatible *in vitro*.

Keywords: Brain biomimicry; SDF-1α controlled release; porous scaffold; aerogel sponges; silk fibroin.

1. Introduction

Efficient three-dimensional (3D) scaffolds serving as cell supports and tissue bridges demand composition and properties tailored to each specific target tissue and purpose. In the case of neural tissue, brain mimicking may help improving scaffolds for not only regenerative purposes (Boni, Ali, Shavandi, & Clarkson, 2018; Dehqan Niri, Karimi Zarchi, Ghadiri Harati, Salimi, & Mujokoro, 2019; Orive, Anitua, Pedraz, & Emerich, 2009) but also for localized treatments, such as brain cancer management through environmental traps that control the progression of the disease (Haji Mansor et al., 2018; Najberg, Haji Mansor, Boury, Alvarez-Lorenzo, & Garcion, 2019). Brain damage might cause cognitive, behavioral and physical disabilities. Depending on the cause, treatments exist to control the damages or slow down the deterioration of the brain. Unfortunately, there is none reconstructive intervention available and the central nervous system (CNS) has limited capacity to spontaneously regenerate. It is therefore necessary to develop innovative strategies to promote tissue repair. One strategy consists in the incorporation to a scaffold of molecules that can attract and support integration of endogenous neural progenitor/stem-cells (NPSCs) to the site of implantation. SDF-1α, also known as CXCL12, is a chemokine that has been pointed out as a potent candidate to improve outcomes in brain injuries due to its well-described involvement in NPSCs homing (Christie & Turnley, 2013; Imitola et al., 2004). However SDF-1α bolus administration in the brain leads to poor results in the long term because of its rapid clearance (Dutta et al., 2017). Encapsulating this chemokine in nanoparticles or immobilizing it in scaffolds may prevent premature degradation and may provide sustained release for NPSCs attraction (Addington et al., 2015; Dutta, Fauer, Mulleneux, & Stabenfeldt, 2015; Jian et al., 2018). SDF-1α has also been shown to accelerate the healing in a variety of other tissues, but prolonged levels of this chemokine are not easy to provide (Hu et al., 2018; Lau & Wang, 2011; Rabbany et al., 2010; Zhao, Jin, Li, Qiu, & Li, 2017).

The 3D scaffold itself should be adequately designed in terms of architecture and physicochemical properties. The brain is made up of 80% water and has a Young's modulus of less than 1 kPa (De Souza & Dobbing, 1971; Engler, Sen, Sweeney, & Discher, 2006; Nava, Raimondi, & Pietrabissa, 2012). Aerogel sponges that can transform into soft hydrogels once hydrated are good candidates to mimic these features; indeed, hydrogel-like bioscaffolds have been pointed out as ideal ones for brain regeneration (Modo, 2019). The scaffold should be designed with pores that are small enough to support 3D cell-cell contacts and large enough to allow good diffusion of nutrients, oxygen and bioactive factors for cell survival and growth. Pore sizes between 20 and 160 µm have been identified as adequate for cell growth and colonization (Mahumane, Kumar, Du Toit, Choonara, & Pillay, 2018). In this context, freeze-dried sponges are promising scaffolds for soft tissue regeneration including the neural one as they can mimic soft tissues peculiarities (Führmann, Obermeyer, Tator, & Shoichet,

2015; Haring et al., 2019; Seyedhassantehrani, Li, & Yao, 2016). Specifically, compared to more compact sponges, aerogel-based nanostructured sponges are characterized by their lightweight and interconnected open porosity, with a texture particularly suitable for cell attachment (Garcia-Gonzalez et al., 2019).

HA is one of the main constituents of the brain extracellular matrix (ECM) (Rouslahti, 1996). It is known to enhance cell mobility and invasion by interacting with the CD44 receptor (Bellail, Hunter, Brat, Tan, & Van Meir, 2004). The main concern with HA as a scaffold is its quick degradation *in vivo*. Differently, SF from the silk worm *Bombyx mori* is known for its biocompatibility, relatively slow degradability and versatile processing abilities (Mobini et al., 2016; Thurber, Omenetto, & Kaplan, 2015; Vepari & Kaplan, 2012). Based on its unique mechanical properties that feature good strength and elasticity, it is possible to produce hydrogels, sponges, films and nanofibers via several organic solvent-free processes (Rockwood et al., 2011). Relevantly, SF has shown low immunogenicity and excellent compatibility with brain, promoting reparative mechanisms (González-Nieto, Fernández-García, Pérez-Rigueiro, Guinea, & Panetsos, 2018; Martín-Martín et al., 2019). Like HA, heparin (hep) is another component of the ECM present in the brain. Due to its strong capacity to bind chemokines, the incorporation of this molecule in a scaffold has been shown to facilitate the loading of SDF-1α (Krieger et al., 2016; Prokoph et al., 2012).

The present work relies on the hypothesis of that suitable combinations of HA, SF and hep may render 3D aerogel scaffolds with synergic features in terms cell infiltration (HA), textural and mechanical properties (SF) and control of SDF-1α uptake and release (hep) avoiding premature clearance. The aim is to obtain mid-term stable scaffolds that can attract cells through the creation of a SDF-1α gradient. To carry out the work, miscibility of HA with SF was first evaluated under different processing conditions due to the reported phase-separation problems found between SF and polysaccharides (Chen, Li, & Yu, 1997; Garcia-Fuentes, Giger, Meinel, & Merkle, 2008). Then, sponges were prepared by the crosslinking of the polymers with N-(3-dimethylaminopropyl)-N'-ethylcarbodiimide hydrochloride (EDC) and N-hydroxysulfosuccinimide sodium salt (NHS) followed by freeze-drying. Aerogel sponges architecture and physicochemical characteristics (porosity, degradation, water uptake and stiffness) were measured as well as their cytocompatibility and *in vitro* release profile of SDF-1α under *in vivo* mimicking conditions.

2. Materials and methods

2.1. Materials

Hyaluronic acid (HA) with a mean molecular weight of 360 kDa (200-400 kDa range), glucuronic acid 47.4% and intrinsic viscosity 7.7 dL/g was supplied by Guinama (Valencia, Spain). Poly-L-lysine (PLL)

with a molecular weight of 150-300 kDa (0.1% w/v in H_2O) was purchased from Sigma-Aldrich (St Louis, MO, USA). Heparin sodium salt (hep) from porcine intestinal mucosa with a molecular weight of 15,000 ± 2,000 Da was purchased from Calbiochem (Billerca MA, USA). HEPES buffer, bovine serum albumin (BSA), resazurin, hyaluronidase from bovine testes type I-S, heparinase I and III blend from *Flavobacterium heparinum* (50 U) and sodium chloride were purchased from Sigma-Aldrich (St Louis, MO, USA). EDC and NHS were from Acros Organics (New Jersey, USA). Human SDF-1α labelled with AlexaFluor647 (AF-SDF-1α) was purchased from Almac Sciences (Craigavon, Northern Ireland). Human SDF-1α was purchased from Miltenyi Biotec (Paris, France).

2.2. Silk fibroin solution preparation and characterization

Solution of SF in water was produced by IMIDA (Murcia, Spain) under GMP conditions. Cocoons of the silkworms *Bombix mori* (reared in IMIDA, Murcia, Spain) were chopped into 4 pieces then boiled in a 0.02 M Na_2CO_3 aqueous solution for 30 minutes to remove the sericin protein. Fibers were rinsed 3 times in distilled water and dried at RT for 3 days. They were dissolved in a 9.3 M LiBr solution for 3h at 60°C to generate a 20% (w/v) solution which was then dialyzed against distilled water for 3 days at 4°C (Snakeskin Dialysis Tubing 3.5 KDa MWCO, Thermo Scientific). The obtained 8% (w/v) SF solution in water was stored at 4°C for less than 1 month.

SF was characterized using SDS-poly(acrylamide) gel electrophoresis (SDS-PAGE) as follows. A SF stock solution at 10 mg/mL was prepared in water and diluted in 5x Laemmlie buffer (90 mmol of 0.5M Tris-HCl, pH 6.8, 20% glycerol, 4% SDS, 0.004% bromphenol blue and 10% β-mercaptoethanol) to obtain a final concentration of 6.25 µg/µL and boiled at 95°C for 5 min. An aliquot (10 µl) was added into the wells. Electrophoresis was performed using a 4-20% gradient mini-protean TGX precast gel (Bio Rad). HiMark Pre-stained protein standards (Thermo Fisher) served as molecular weight marker. After electrophoresis, the gel was stained with solution 1% (w/v) Coomassie Brilliant Blue R- 250, 10% (v/v) acetic acid, 40% (v/v) methanol and distilled water over night, and destained with 10% (v/v) acetic acid, 40% (v/v) methanol and distilled water for 5h. Three different batches were analyzed.

2.2. Films preparation and characterization

Dispersions of HA 4% (w/v), SF 4% (w/v) or SF 4% (w/v) with HA 2% (w/v) in HEPES buffer (C_{HEPES}= 20.10^{-3} M, C_{NaCl} = 0.15 M, pH = 7.4) were prepared under magnetic stirring for either 15 min, 2 h or 15 h. Films were prepared by pouring the dispersions in Petri dishes and left to dry 24 h at RT. Films morphology was observed by scanning electron microscopy (SEM) with a SEM Evo LS15 (Zeiss, USA) after being coated with iridium.

2.3. Aerogel sponges preparation and characterization

2.3.1 Aerogels preparation

HA was dissolved in HEPES buffer (C_{HEPES} = $20 \cdot 10^{-3}$ M, C_{NaCl} = 0.15 M, pH=7.4) to obtain a final concentration of 4% (w/v). Sponges were prepared with 4 different compositions by first mixing the polymers together: HA 4% (w/v) with PLL 0.01% (w/v) (HA-PLL), SF 4% (w/v) (SF), SF 4% (w/v) with HA 2% (w/v) (SF-HA), and SF 4% (w/v) with HA 2% (w/v) and hep 1% (w/v) (SF-HA-hep). For the preparation of the SF-HA and the SF-HA-hep sponges, SF 8% (w/v) solution was gently stirred 5h with an equivalent volume of HA 4% (w/v) solution in HEPES buffer with or without heparin sodium salt. EDC and NHS were dissolved in H_2O (C_{EDC} = 50 mg/mL, C_{NHS} = 18 mg/mL) and then immediately added to the HA-PLL or SF-HA solution with a 1:10 (crosslinkers/polymers, v/v) ratio and mixed rapidly. For the SF-HA-hep, a higher concentration of crosslinker was needed (C_{EDC} = 150 mg/mL, C_{NHS} = 55 mg/mL). The solutions were poured immediately in a 96-well plate, covered and allowed to crosslink for 15 h at 4°C. The gels were then frozen at -20°C for 24 h, and freeze-dried in a Telstar® LyoQuest at -70°C and 0.01 mBar overnight. After freeze-drying, the aerogel sponges were removed from the wells and stored in a desiccator with silica gel. For aerogels containing SF, an annealing step was applied to increase the crystallinity of the protein in order to obtain sponges that maintain their structural integrity in aqueous solutions (Hu et al., 2011). Annealing with ethanol vapor consisted in placing the sponges in a desiccator at atmospheric pressure with ethanol 70% (v/v) at the bottom and kept for 2 h at RT. The sponges were then freeze-dried again to remove traces of ethanol.

2.3.2 Fluorescence microscopy of internal structure of the aerogel sponges

Sponges were frozen in liquid nitrogen and immobilized in Tissue-Tek® (Sakura, USA). Cross sections with 30 µm thickness were obtained using a cryostat® (Leica CM3050 S Research Cryostat, Leica Biosystems Nussloch GmbH, Germany). Sections were placed on Starfrost® slides coated with gelatin and chrome alum, incubated 5 min with ActinRed (ThermoFisher), and the lamella mounted on the sections with fluorescence mounting medium (Dako, Agilent Technologies, USA). Finally, the slide was observed under a fluorescence microscope (Carl Zeiss Axioskop 2 MOT, Germany) with a rhodamine filter, and pictures were taken with the same exposition time of 58 ms between slides.

2.3.3 FTIR analysis

Attenuated total reflection Fourier transformed infra-red (ATR-FTIR) analysis of sponges (10 mg) was performed with a Gladi-ATR equipped with a diamond crystal (Pike, Madison, WI, USA). For each measurement, 64 scans were recorded with a resolution of 4 cm^{-1}, and the wavelength ranged from 400 to 4000 cm^{-1}. The increase in crystallinity of SF sponges after ethanol annealing was evaluated in terms of percentage of β-sheets applying the method described by Hu *et al.* (Hu, Kaplan, & Cebe,

2006). Briefly, Fourier self-deconvolution (FSD) of the IR spectra covering the amide I region (1595-1705 cm^{-1}) was performed using Opus 7.8 software (noise reduction factor of 0.3 and bandwidth of 2.5) followed by a curve fitting on this region. Peaks at 1616-1621, 1622-1627, 1628-1637, and 1697-1703 corresponded to β-sheets (Hu et al., 2006).

2.3.4 Porosity evaluation

Density and porosity (P) of aerogel sponges was calculated using Eq. (1) and Eq. (2). The thickness and diameter of the specimens were measured using a digital caliper. Polymer density was supposed to be equal to 1. For each composition, three sponges were measured.

$$Sponge\ density\ (g.cm^{-3}) = \frac{Sponge\ mass\ (mg)}{Sponge\ volume\ (mm^3)} \quad \text{Eq. (1)}$$

$$P\ (\%) = \left(1 - \frac{Sponge\ density\ (g.cm^{-3})}{Polymer\ density\ (g.cm^{-3})}\right) \times 100 \quad \text{Eq. (2)}$$

2.3.5 Water uptake

The capability of the sponges to uptake water was evaluated, in triplicate, after immersion at RT in 3 ml of NaCl 0.9%. The sponges were withdrawn using tweezers, gently treated with blotting paper for 10 s to remove the unabsorbed excess of medium, weighed, and immediately returned to the corresponding vial. The weight measurements were repeated until the hydration equilibrium was reached. Water uptake was calculated as follows:

$$Water\ uptake\ (\%) = \left(\frac{hydrated\ sponge\ (mg) - dry\ sponge(mg)}{hydrate\ sponge\ (mg)}\right) \times 100 \quad \text{Eq. (3)}$$

2.3.6 Young's modulus measurement

Hydrated sponges were cut to obtain cylinders with a thickness of about 3 mm. The cylinders were placed on the platform of a texture analyzer (TA.TX Plus, Texture Technologies, USA) and compressed downward up to 1.5 mm with a speed of 1 mm/s. Three hydrated sponges were analyzed for each composition. The Young's modulus was determined from the slope of the curve obtained by plotting the force (F) needed to compress the sponge divided by the cross-sectional area of the sponge (S) against the deformation of the sponge (ΔL) divided by the initial length of the sponge (L) (Lassoued, Delarue, Launay, & Michon, 2008) as follows

$$E\ (MPa) = \frac{F\ (N)/S\ (mm^2)}{\Delta L\ (mm)/L\ (mm)} \quad \text{Eq. (4)}$$

2.3.7 Degradation

In vitro erosion of sponges was monitored, in triplicate, in PBS with enzymes (0.3 mg/mL hyaluronidase (Correia et al., 2011) and 0.1 U/mL heparinase) at 37°C for 7 and 21 days. Aerogel sponges were cut to have similar sizes (6 mm diameter and 3 mm height) and weighed. After 7 or 21 days in 3 mL medium, the sponges were washed with water, snapped frozen in liquid nitrogen and then freeze-dried. Sponge degradation was calculated as percent of mass loss (aerogel sponge mass-degraded sponge mass) referred to the original aerogel sponge mass.

2.3.8 Scanning electron microscopy (SEM)

Sponge morphology (surface and transversal cut) was observed using a SEM Evo LS15 (Zeiss, USA). Sponges were firstly hydrated in NaCl 0.9% (w/v) aqueous solution then, either directly or after 7 days at 37°C, snapped frozen in liquid nitrogen. Pore diameter was measured using ImageJ 1.50 software; at least 94 pores were measured per sponge.

2.4. Cytocompatibility

The cytocompatibility was evaluated using human fibroblast cells (NIH/3T3, ATCC® CRL-1658™) that were cultured at 37°C and 5% CO_2 in DMEM high glucose media (Sigma Aldrich) supplemented with 10% fetal bovine serum, and 1% penicillin/streptomycin and subcultured every 3-4 days. Cells were seeded in a 24-well plate (20,000 cells/well) for 24 h. Hydrated HA-PLL, SF, SF-HA and SF-HA-hep sponges in PBS were firstly cut to obtain cylinders with 2 mm height and then sterilized under UV light for 1 h. Immediately before use, sponges were washed 3 times with PBS under sterile conditions and then equilibrated in complete DMEM for 15 min. Suspended culture inserts (MilliCell, PET, 8 µm) were placed in the wells with sponges inside in triplicate. Inserts without sponges were used as control. After 24 h of incubation at 37°C and 5% CO_2, inserts and sponges were removed, and the media was replaced with 500 µL of resazurin 44 µM. After 2 h of incubation at 37°C, cell viability was estimated from the fluorescence intensity of the reduced product of resazurin, called resorufin, which is formed in the cytosol of viable cells. Fluorescence was measured using a ClarioStar microplate fluorometer (BMG Labtech GmbH, Ortenberg, Germany) at λ_{ex} = 545 nm and λ_{em} = 600 nm. All readings were normalized to those obtained with the control wells.

2.5. Analysis of SDF-1α uptake and release

2.5.1. Distribution of SDF-1α in the sponges

SF-HA and SF-HA-hep sponges were washed in PBS (as in 2.4) and cut to obtain cylinders of 2 mm height and 3 mm diameter. Excess of PBS was removed with Nunc paper. A drop of 3 µL of AF-SDF-1α (300 ng in PBS) was added on top of the sponges, which were then incubated 1h at 4°C. A map of the

fluorescence of the sponges (λ_{ex} = 625 nm; λ_{em} = 680 nm) was performed with a spectrophotometer (CLARIOstar®plus, BMG Labtech, Orthenberg, Germany). Each point was measured 500 µm apart.

2.5.2. Quantitative analysis of SDF-1α

SF-HA and SF-HA-hep sponges were hydrated and cut as above (section 2.5.1). Then, the sponges were placed in Eppendorf tubes coated beforehand with Sigmacote® (Sigma-Aldrich, USA) and sterilized 1h with UV light before adding 3 µL of SDF-1α (300 ng in PBS) on top of the sponges. The sponges were incubated for either 1 h or 12 h at 4ºC. PBS (500 µL) with 0.1% BSA and enzymes (0.3 mg/mL hyaluronidase and 0.1 or 0.5 U/mL heparinase) was added in each tube and incubated at 37°C under gentle oscillation. At least three sponges of each composition were tested for each different loading/release condition. The release medium was collected at defined time points (1 h, 8 h, 1 d, 2 d, 3 d and 7 d) and an equal volume of fresh medium was added back to the sponges. All solutions were collected and frozen at -20°C until ELISA tests (R&D Systems, Lille, France)

2.6. Statistical analysis

The data were statistically analyzed using an ANOVA test with Prism 7 software. In all statistical comparisons $p < 0.05$ was considered statistically significant.

3. Results and Discussion

3.1. Silk fibroin characterization

In the gland of *Bombix mori*, SF is composed of heavy molecular weight chains (H-chains) of about 370 kDa) and light molecular weight chains (L-chains) of about 25 kDa (Yamada, Nakao, Takasu, & Tsubouchi, 2001). Depending on the process used to obtain the SF solution, SF can be more or less degraded, which may have an impact on the properties of the materials produced (Nultsch & Germershaus, 2017). The molecular weight profile of the SF obtained under GMP conditions by IMIDA was evaluated by means of SDS-PAGE with a 4-20% gradient gel (Figure 1). The L-chain at 25 kDa was clearly observed. The H-chain was recorded between 238 kDa and 460 kDa. These results confirm that the process used to produce the SF solution was able to retain the integrity of the protein.

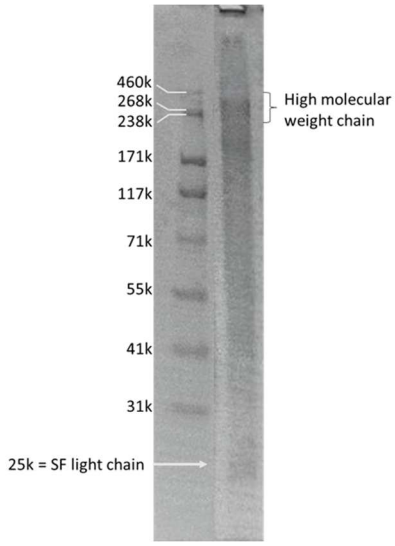

Figure 1: Molecular weight analysis of the SF solution by SDS-PAGE showing the expected difference in electrophoretic mobility between the high molecular weight protein and the low molecular weight protein.

3.2. Kinetic study of the interaction of SF with HA

Homogeneous dispersions of SF with hydrophilic polymers such as HA have been previously shown to be quite difficult to attain. Phase separation and/or specific interactions are quite prone to occur (Garcia-Fuentes et al., 2008; Garcia-Fuentes, Meinel, Hilbe, Meinel, & Merkle, 2009). Thus, the effect of the mixing time on the inner structure of SF-HA systems was investigated by preparing films composed of either HA, SF or a blend of SF and HA that had been stirred for 15 min, 2 h or 15 h (Figure 2). The HA film displayed a rough surface while the SF film was reproducing the petri dish pattern. When mixed together for 15 min, two separate phases appeared in the form of globules with sizes ranging from 9.6 to 128.2 µm (38.7 ± 23.5 in average) that were clearly outlined by the second phase. The phase inside the globules had a similar topography to that of the SF film while the other phase appeared to be similar to that of the HA film. After 2 h stirring, the globules became smaller (2.4 – 19 µm), resulting in an increase in homogeneity. After overnight mixing, the film adopted a much more homogeneous appearance. However, large aggregates could be seen to form extensively across the surface of the film. Therefore, an intermediate mixing time of about 5h for applied for sponge preparation.

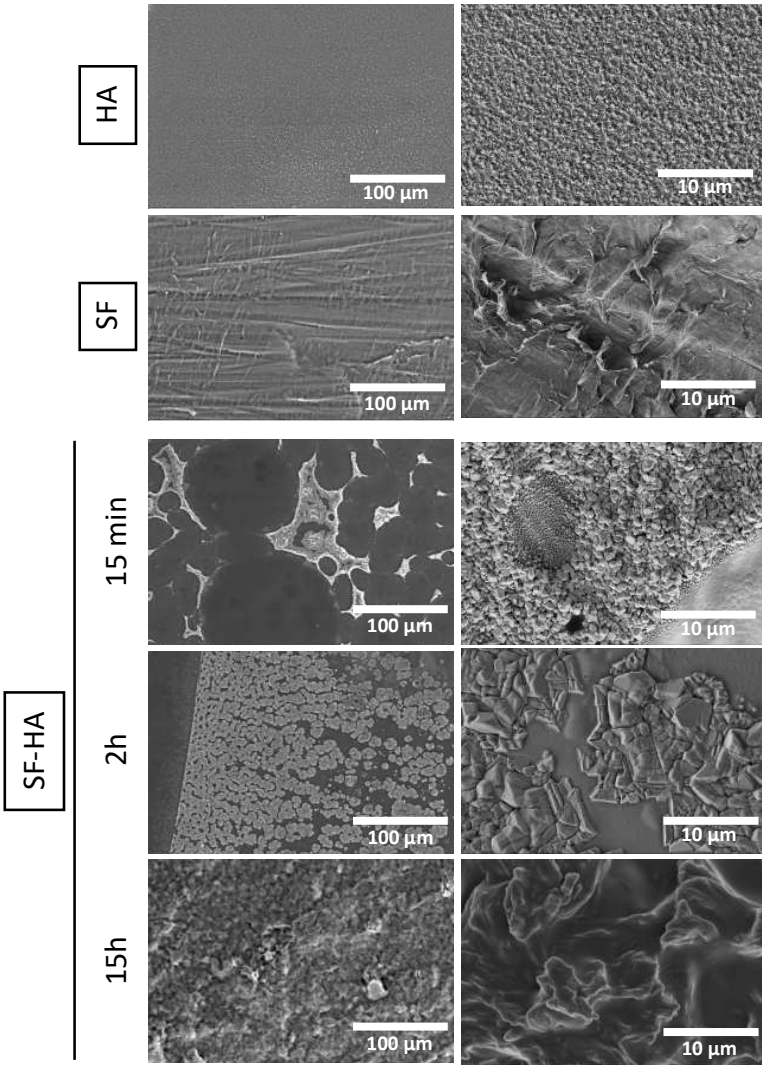

Figure 2: SEM images of films prepared with either HA, SF or a blend of SF and HA mixed for 15 min, 2h or 15h.

3.3. Structural characterization of the aerogel sponges

HA-PLL, SF, SF-HA and SF-HA-hep aerogel sponges were prepared by crosslinking of the polymers followed by freeze-drying. A mixture of HA and PLL (only 0.01% w/v) was used instead of HA solely since the reaction with EDC and NHS requires a carboxylate and a primary amine (Kuo, Swarm, & Prestwich, 1991). Carboxylate moieties are present on the HA chains but not the amine groups. Therefore, this crosslinking reaction does not proceed well for HA solely. It is known that PLL facilitates cellular adhesion via electrostatic interactions and may improve HA performance in this regard (Mazia, Schatten, & Sale, 1975), but the proportion of PLL was kept low to facilitate comparisons with the other sponges.

The microstructure of the aerogel sponges' walls was observed under fluorescence microscopy (Figure 3). Antibodies used in immunofluorescence imaging like DAPI or ActinRed fixed in a non-

specific manner to SF without interacting with HA. Indeed, a much stronger signal was observed for the SF sponge compared with the HA-PLL sponge. The walls of the SF sponge showed a smooth surface. Upon the addition of HA, the walls of the pores of SF-HA sponge became irregular and seemed to be formed by small fluorescent aggregates. Such aggregates were intensified upon the introduction of hep. The structure of SF-HA and SF-HA-hep aerogel sponges was formed by fluorescent aggregates that should therefore be SF-rich domains distributed in a non-fluorescent matrix composed mainly of HA. Garcia-Fuentes *et al.* (2008) have previously reported that SF/HA mixtures at 80:20 and 60:40 weight ratios may develop phase separation, with one phase containing HA alone while the other phase consisted of a mixture of HA and SF. The phase separation observed in the films prepared by us (SF/HA 2/1 ratio) as well as the structure observed in the pore walls of the aerogel sponges are consistent with those previous findings. We can therefore pointed out that the polymer ratio as well as the mixing time are critical parameters when SF and HA are used to prepare 3D scaffolds.

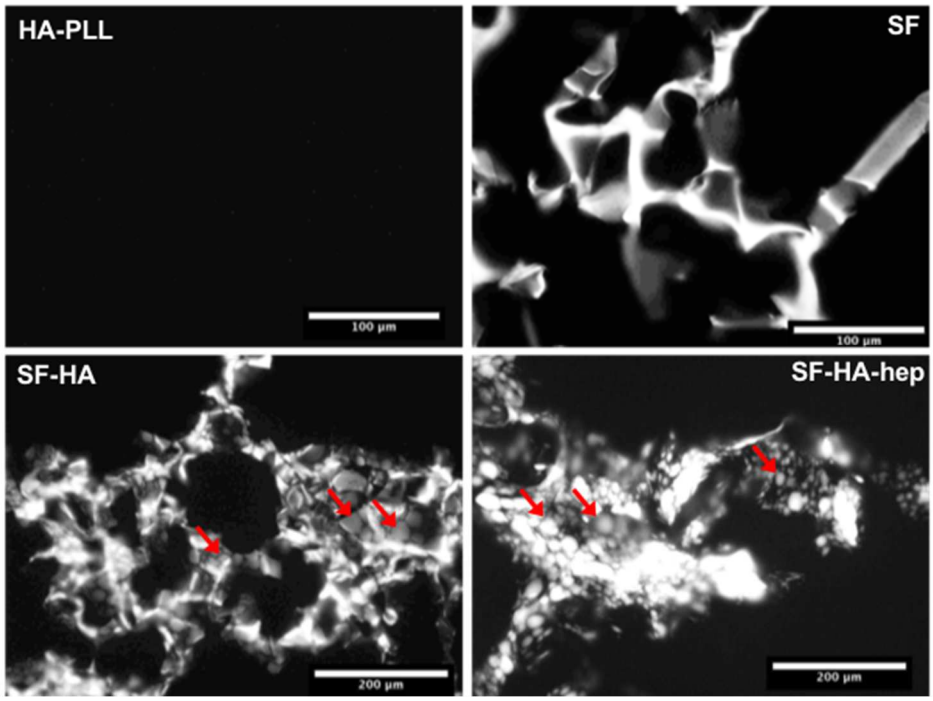

Figure 3: Autofluorescence of the aerogel sponges under Rhodamine filter with the same exposure time of 58 ms. Red arrows indicate the presence of aggregates.

ATR-FTIR analysis was performed on the aerogel sponges before and after ethanol annealing to observe the changes in crystallinity (Figure 4). After ethanol annealing, a shift from 1640 cm^{-1}, which corresponds to SF random coils, to 1621 cm^{-1}, which corresponds to SF β-sheets (Hu et al., 2006), was observed for all the sponges with SF. All annealed sponges had a similar β-sheet content of about

28%. Without the annealing step, the structure of the sponges collapsed after a few minutes in an aqueous environment.

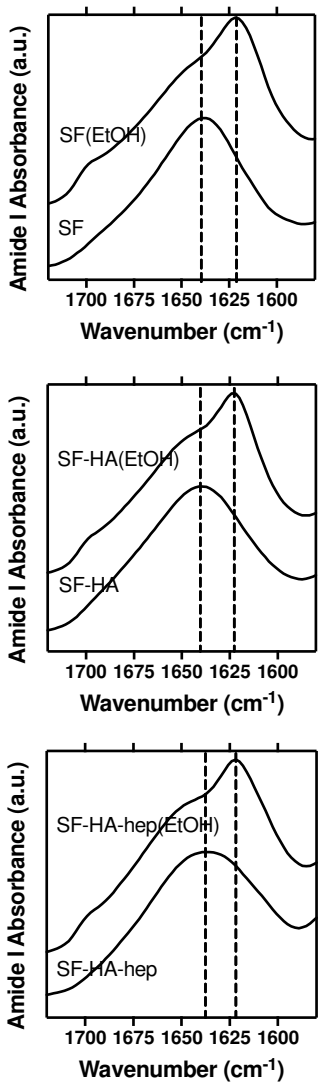

Figure 4: FTIR absorbance spectra in the amide I region for aerogel sponges containing SF before and after ethanol annealing. Peak at 1621 cm^{-1} is typical of the β-sheet conformation of SF, while the peak at 1640 cm^{-1} corresponds to SF random coils.

All aerogel sponges exhibited high porosity, ranging from 82% for the SF-HA-hep sponge to 93% for the SF sponge (Table 1), which inversely correlated with the content in solids used to prepare the starting dispersion (described in section 2.3.1.). The capability of the sponges to uptake water when immersed in NaCl 0.9% (w/v) aqueous solution was of 93% for SF-HA-hep and SF-HA sponges, and 95% for HA-PLL sponge (Table 1). Similarities in water uptake may be related to similar porosity and hydrophilicity. Degradation was monitored at 37°C during 7 and 21 days in PBS supplemented with hyaluronidase and heparinase at concentrations that mimic *in vivo* conditions (Correia et al., 2011; Frost, Csoka, Wong, & Stern, 1997) (Figure 5A). HA-PLL sponges were completely degraded after 7

days and produced a clear solution, while SF sponges maintained their integrity even after 21 days. SF-HA and SF-HA-hep showed intermediate degradability. An ideal scaffold for brain regeneration should be biodegradable to avoid the need for secondary surgery to remove the implant. Simultaneously, the degradation rate of the scaffold should match the rate of tissue reconstruction so that the newly formed tissue does not collapse before the regeneration process is complete. Too slow degrading scaffolds may compromise tissue regeneration, as previously reported for hydrogel-based brain bioscaffolds (Modo et al., 2019) and SF-based bone scaffolds with tunable degradability (Park et al., 2010). Therefore, intermediate degradation rates (in the frame of days) have been pointed out as preferable (Park et al., 2010; Modo et al., 2019). In good agreement with previous reports, the mass loss in scaffolds composed of HA and SF blends can be attributed to the degradation of HA (Garcia-Fuentes et al., 2009). Since HA degrades quicker than SF, the matrix has to be as homogeneous as possible to avoid the generation of scaffolds with distinct HA-rich compartments susceptible to rapid *in vivo* decomposition.

Table 1: Porosity of the aerogel sponges, water uptake in NaCl 0.9% aq. solution, and Young's modulus after hydration.

Sponge	Porosity (%)	Water uptake (%)	Young's modulus (kPa)
HA-PLL	91.9 ± 1.9	95.5 ± 0.2	6.0 ± 1.6
SF	92.7 ± 0.6	93.2 ± 0.5	21.7 ± 1.6
SF-HA	87.4 ± 1.0	92.8 ± 2.1	12.5 ± 7.8
SF-HA-hep	82.3 ± 2.2	92.9 + 2.2	13.1 ± 5.1

To confirm these results, the morphology of the aerogel sponges was observed using SEM before and after 7 days in PBS without enzymes at 37°C (Figure 5B-C). These study conditions were selected to induce intermediate degradation of the HA-PLL sponge. At the end of this study, signs of degradation in the form of thinner walls and larger pores were clearly visible in HA-PLL sponges. Sponges made of SF and HA mixtures showed excellent preservation of morphology, confirming that the addition of SF to the sponges allows for retention of the aerogel structure in aqueous medium. SEM images revealed good pore connectivity and an average pore size between 30 ± 13 µm for SF-HA and 87 ± 29 µm for SF. The structure of these porous sponges resembles the one of the brain ECM, which has been described as a foam-like structure (Nicholson & Syková, 1998). The pores were of various sizes ranging from 20 to 140 µm across the different sponge compositions designed in the present work. This size range can be considered adequate since the pores are sufficiently small to support 3D cell-cell contacts, but large enough to allow good diffusion of nutrients, oxygen and bioactive factors for

cell survival and growth (Mahumane et al., 2018). The ideal porosity was defined to be around 90% (Jurga et al., 2011).

Texture analysis was performed on hydrated sponges and Young's modulus was calculated (Table 1). The values of Young's modulus recorded ranged from 6 kPa for HA-PLL to 22 kPa for SF. Sponges made from mixtures of SF and HA showed intermediate values. The brain has Young's modulus close to or below 1 kPa (Engler et al., 2006; Nava et al., 2012) although the stiffness varies depending on the brain region (white matter stiffness is higher and increases with the content in myelin (Weickenmeier et al., 2016)) and the pathology, increasing in cancer and decreasing in Alzheimer´s disease (Murphy et al., 2011; Wang, Tong, & Yang, 2014). It is still quite challenging to produce scaffolds that maintain their structural integrity with a Young's modulus as low as the one of the brain. Most of previous bio-stable scaffolds reported, even those also containing SF, are stiffer than the sponges developed herein (Wentao et al., 2019). Thus, the aerogel sponges combine stiffness close to those of brain while they are easy to handle and could be conveniently cut into the desired dimensions to fit the lesion gap at the intended site of implantation.

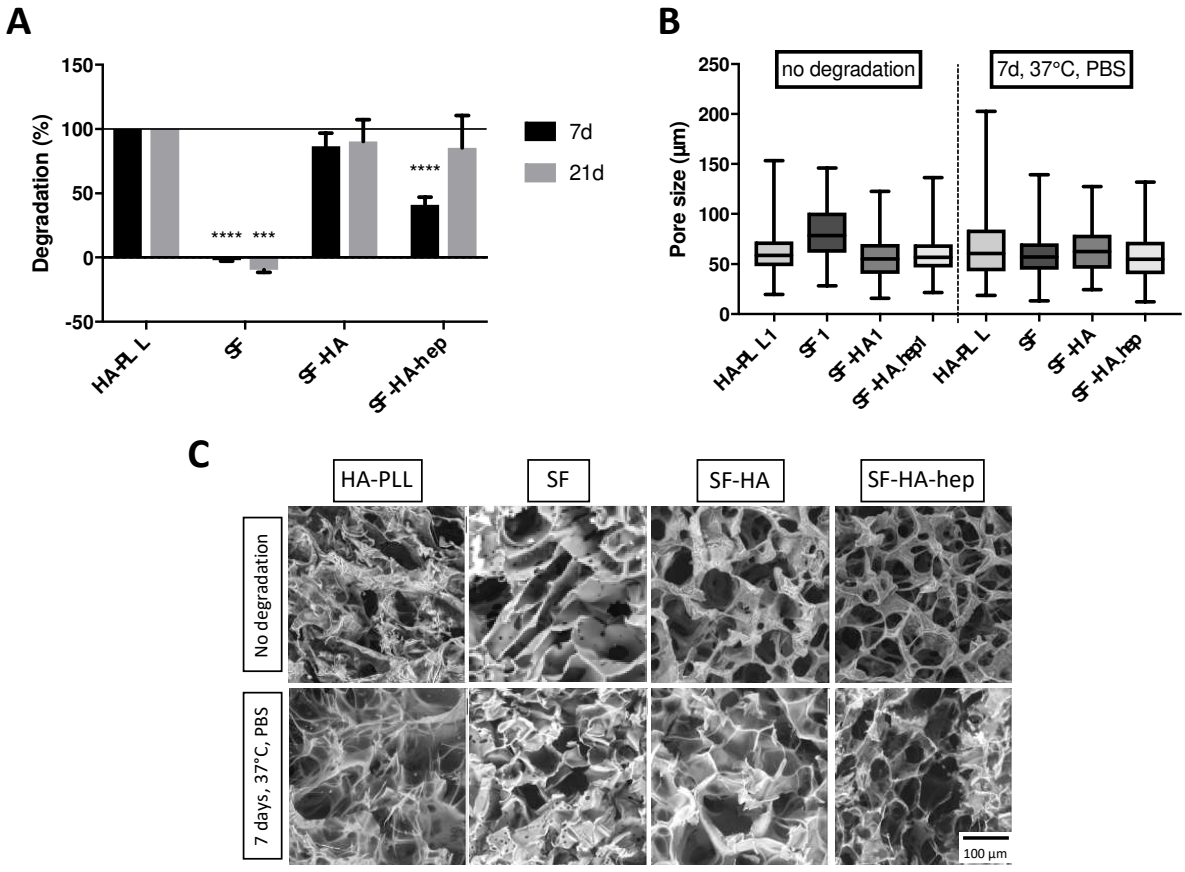

Figure 5: (A) Degradation of HA-PLL, SF, SF-HA and SF-HA-hep aerogel sponges in PBS with enzymes (hyaluronidase and heparinase) at 37°C for 7 and 21 days. Paired comparisons were conducted between degradation of HA-PLL and the others with the same conditions. (B) Average pore size

before and after incubation of the sponges for 7 days in PBS without enzymes at 37°C. At least 94 pores were measured per sponge. (C) SEM images of sponges; scale bar 100 µm. ANOVA: ***p<0.001, ****p<0.0001.

3.3. Cytotocompatibility

The cytocompatibility of the sponges was tested, via the indirect and direct contact methods, against the NIH/3T3 mouse fibroblast cell line which is considered as highly sensitive to any scaffold-induced toxicity (Xia et al., 2008). The HA-PLL, SF, SF-HA and SF-HA-hep sponges showed no discernible cytotoxicity with both methods (Figure 6) although the viability slightly decreased for the SF-HA-hep sponge with the direct contact method (76 ± 9% viability), but it was not statistically significant. These preliminary tests suggest good cytocompatibility although further studies with several other cell lines and other metabolic activity assays would be required before in vivo testing.

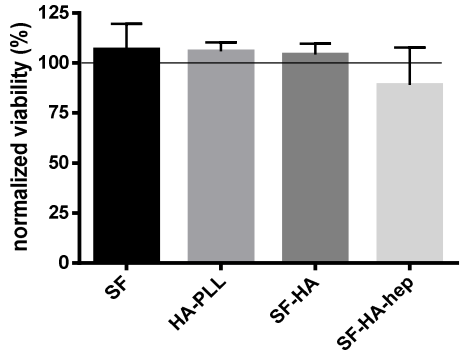

Figure 6: Evaluation of the compatibility of SF, HA-PLL, SF-HA and SF-HA-hep aerogel sponges with NIH/3T3 cells.

3.4 SDF-1α uptake and release

Since the SF-HA and SF-HA-hep sponges provided a good trade-off between the low rigidity of the HA-PLL sponge and the slow degradation of the SF sponge, they were chosen for the SDF-1α uptake and release studies.

SDF-1α dissolved in PBS was dropped on the SF-HA and SF-HA-hep sponges. The distribution profile of the protein inside the sponge was visualized using SDF-1α coupled to AlexaFluor 647. A fluorescence map was subsequently obtained (Figure 7). After 1 h incubation, the protein formed a radial concentration gradient from the center (where the drop was deposited) toward the edges of the sponges. Since it has been described that CXCR4 receptor-bearing cells can migrate in response

to an SDF-1α concentration gradient, the radial distribution of SDF-1α in the sponge may be beneficial in facilitating extensive infiltration of stem cells into the sponge for tissue regeneration (Imitola et al., 2004) as well as for other applications that require the cells to be confined in a matrix (Najberg et al., 2019).

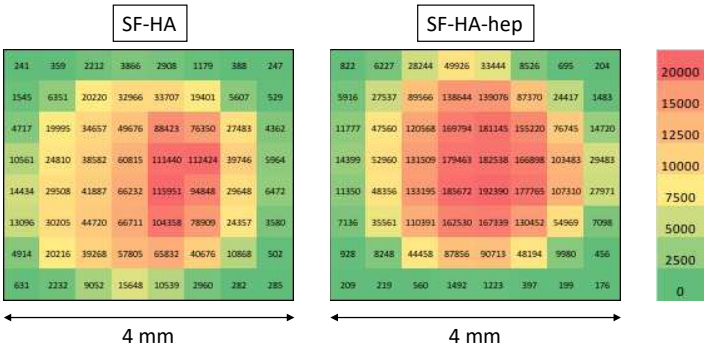

Figure 7: Distribution of AF-SDF-1α in the SF-HA and SF-HA-hep aerogel sponges recorded via fluorescence detection. Numbers represent the fluorescence intensity at each point. Fluorescence maps showed here are representative of n=3.

For the release studies, SDF-1α was dropped onto the SF-HA and SF-HA-hep sponges and then the systems incubated for 1 h or 12 h in order to investigate whether the time of incubation may alter the interactions strength of the chemokine with the sponge components. SDF-1α release was recorded in PBS with enzymes (hyaluronidase and heparinase) at 37°C over 7 days (Figure 8). The concentration of hyaluronidase was fixed at 0.3 mg/mL, but heparinase was tested at two different levels, 0.1 and 0.5 U/mL, to cover a wide range of physiological conditions (Correia et al., 2011; Frost, Csoka, Wong, & Stern, 1997). For the SF-HA-hep sponge, a maximum release of 2.1 ± 0.8% and 4.0 ± 0.6% was reached after 3 days in the release medium prepared with 0.1 and 0.5 U/mL heparinase, respectively. Therefore, an increase in enzyme promoted the release although the sponges maintained their integrity, which means that enzyme only altered the heparin moieties. It is expected that, *in vivo*, the release continues over time in parallel with the degradation of the sponge. Differently, SF-HA sponge showed a marked burst in the first hours, releasing 22 ± 10% and 10 ± 8% after 2 days in the release medium prepared with 0.1 and 0.5 U/mL heparinase, respectively. As expected these sponges were not sensitive to the increase in heparinase concentration, and the slower release observed in 0.5 U/mL heparinase medium may be related to the more prolonged incubation of the sponges with SDF-1α during loading (12 h instead of 1 h). SDF-1α is a positively charged protein at physiological pH (isoelectric point (IEP) ~9.6) while HA and SF are negatively charged (IEP ~2.9 and ~4.6 respectively) (Foo et al., 2006; Malay, Bayraktar, & Batigün, 2007),

allowing the protein to bind to the sponges via electrostatic interactions. In a saline medium, such as PBS with enzymes, the electrostatic interactions become weaker and therefore the release can proceed. The dispersion of the release data points may be due to fragmentation of the SF-HA sponges in pieces of various sizes under the gentle soaking conditions of the release test. Heparin is known to form a strong complex with SDF-1α (Sadir, Baleux, Grosdidier, Imberty, & Lortat-Jacob, 2001), which explains the slower release from the SF-HA-hep sponge. Indeed, the strong SDF-1α retention capacity displayed by the SF-HA-hep sponge has not been reported before to the best of our knowledge (Bladergroen et al., 2009; Hu et al., 2018; Krieger et al., 2016; Prokoph et al., 2012; Purcell, Elser, Mu, Margulies, & Burdick, 2012; Yang et al., 2015).

It should be also noted that, compared to other more sophisticated ways of SDF-1α loading, the SF-HA-hep sponge allowed for simple, direct loading of relatively large amounts of the protein without exhibiting any burst effect. A strong retention of SDF-1α inside the scaffold might be advantageous for attraction of cells towards the core of the scaffold via haptotaxis as well as cell retention over time (Monneau, Arenzana-Seisdedos, & Lortat-Jacob, 2016).

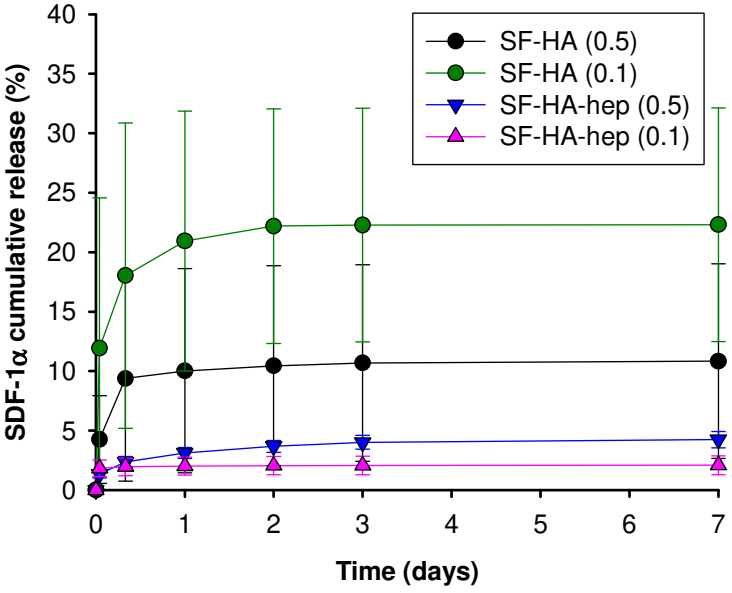

Figure 8: SDF-1α cumulative release from the SF-HA and SF-HA-hep aerogel sponges during 7 days in PBS with enzymes (0.3 mg/mL hyaluronidase and 0.1 or 0.5 U/mL heparinase). Heparinase concentration in the release medium is indicated in the legend. Sponges tested in the medium with the highest heparinase concentration (0.5 U/mL) were previously incubated with SDF-1α for 12 h (blue and black colors). Other sponges were incubated for 1 h (pink and green colors). All values were expressed in percentage of the amount of SDF-1α added to the sponges

4. Conclusion

In summary, cross-linking of mixtures of SF and HA followed by freeze-drying results in aerogel sponges with advantageous properties as soft tissue scaffold compared to those of each biopolymer in separate. The strong autofluorescence of SF allowed for monitoring the homogeneous distribution of the components during sponge preparation and to setup the processing conditions. The SF-HA and SF-HA-hep aerogel sponges exhibited intermediate physicochemical properties (Young's modulus, degradation behaviour) compared to those of SF (~22 kPa; too slow degradation) or HA-PLL(~6 kPa; fast disintegration) sponges. The soft hydrated aerogel sponges showed Young´s modulus as low as those of brain tissue, but maintain their integrity for several days in enzyme-containing physiological-like medium. All sponges showed adequate porosity and pore size to be colonized by cells. Nevertheless, the incorporation of heparin resulted to be critical for the hosting and sustained release of the chemokine SDF-1α. Thus, SF-HA-hep sponges are pointed out as outstanding scaffolds able to uptake relatively large amounts of the protein and prevent burst release for tissue engineering applications.

ACKNOWLEDGEMENTS

This work was supported by the "Institut National de la Santé et de la Recherche Médicale" (INSERM), University of Angers (Angers, France), MINECO (SAF2017-83118-R), Agencia Estatal de Investigacion (AEI, Spain), Fondo Europeo de Desarollo Regional (FEDER), and COST AERoGELS CA18125 European Commission. The work was also supported by the French National Research Agency (ANR) and the National Institute of Health Carlos III (ISCIII), under the frame of EuroNanoMed III (GLIOSILK project). The authors thank also the "Région Pays de la Loire" for fundings in the framework of the project "International strategy NANOFAR+". MN was a Ph.D. student involved in the Erasmus Mundus Joint Doctorate program for Nanomedicine and Pharmaceutical Innovation (EMJD NanoFar). She received a fellowship from "La Région Pays-de-la-Loire". EG and MN were also members of the LabEx IRON "Innovative Radiopharmaceuticals in Oncology and Neurology" as part of the French government "Investissements d'Avenir" program, and of the Cancéropôle Grand-Ouest (tumor targeting and radiotherapy network). The authors acknowledge the help given by R. Varela Calviño (USC) for SDS-PAGE experiments.

REFERENCES

Addington, C. P., Heffernan, J. M., Millar-Haskell, C. S., Tucker, E. W., Sirianni, R. W., & Stabenfeldt, S. E. (2015). Enhancing neural stem cell response to SDF-1alpha gradients through hyaluronic acid-laminin hydrogels. *Biomaterials*, *72*, 11–19. https://doi.org/10.1016/j.biomaterials.2015.08.041

Bellail, A. C., Hunter, S. B., Brat, D. J., Tan, C., & Van Meir, E. G. (2004). Microregional extracellular matrix heterogeneity in brain modulates glioma cell invasion. *International Journal of Biochemistry and Cell Biology*, *36*(6), 1046–1069. https://doi.org/10.1016/j.biocel.2004.01.013

Bladergroen, B. A., Siebum, B., Siebers-Vermeulen, K. G. C., Kuppevelt, T. H. Van, Poot, A. A., Feijen, J., Figdor, C. G., & Torensma, R. (2009). *In vivo* recruitment of hematopoietic cells using stromal cell–derived factor 1 alpha–loaded heparinized three-dimensional collagen scaffolds. *Tissue Engineering Part A*, *15*(7), 1591–1599.

Boni, R., Ali, A., Shavandi, A., & Clarkson, A. N. (2018). Current and novel polymeric biomaterials for neural tissue engineering. *Journal of Biomedical Science*, *25*(1), 1–21. https://doi.org/10.1186/s12929-018-0491-8

Chen, X., Li, W., & Yu, T. (1997). Conformation transition of silk fibroin induced by blending chitosan. *Journal of Polymer Science: Part B: Polymer Physics*, *35*, 2293–2296. https://doi.org/10.1002/(SICI)1099-0488(199710)35:14<2293::AID-POLB9>3.0.CO;2-X

Christie, K. J., & Turnley, A. M. (2013). Regulation of endogenous neural stem/progenitor cells for neural repair—factors that promote neurogenesis and gliogenesis in the normal and damaged brain. *Frontiers in Cellular Neuroscience*, *6*(January), 1–18. https://doi.org/10.3389/fncel.2012.00070

Correia, C. R., Moreira-Teixeira, L. S., Moroni, L., Reis, R. L., van Blitterswijk, C. A., Karperien, M., & Mano, J. F. (2011). Chitosan Scaffolds containing hyaluronic acid for cartilage tissue engineering. *Tissue Engineering Part C: Methods*, *17*(7), 717–730. https://doi.org/10.1089/ten.tec.2010.0467

De Souza, S. W., & Dobbing, J. (1971). Cerebral edema in developing brain : i . Normal water and cation content in developing rat brain and postmortem changes. *Experimental Neurology*, *32*, 431–438.

Dehqan Niri, A., Karimi Zarchi, A. A., Ghadiri Harati, P., Salimi, A., & Mujokoro, B. (2019). Tissue engineering scaffolds in the treatment of brain disorders in geriatric patients. *Artificial Organs*, (February), 1–14. https://doi.org/10.1111/aor.13485

Dutta, D., Fauer, C., Mulleneux, H. L., & Stabenfeldt, S. E. (2015). Tunable controlled release of bioactive SDF-1α via specific protein interactions within fibrin/nanoparticle composites. *Journal of Materials Chemistry B*, *3*(40), 7963–7973. https://doi.org/10.1039/c5tb00935a

Dutta, D., Hickey, K., Salifu, M., Fauer, C., Willingham, C., & Stabenfeldt, S. E. (2017). Spatiotemporal presentation of exogenous SDF-1 with PLGA nanoparticles modulates SDF-1/CXCR4 signaling axis in the rodent cortex. *Biomater. Sci.*, *5*(8), 1640–1651.

https://doi.org/10.1039/C7BM00489C

Engler, A. J., Sen, S., Sweeney, H. L., & Discher, D. E. (2006). Matrix elasticity directs stem cell lineage specification. *Cell*, *126*(4), 677–689. https://doi.org/10.1016/j.cell.2006.06.044

Foo, C. W. P., Bini, E., Hensman, J., Knight, D. P., Lewis, R. V., & Kaplan, D. L. (2006). Role of pH and charge on silk protein assembly in insects and spiders. *Applied Physics A: Materials Science and Processing*, *82*(2), 223–233. https://doi.org/10.1007/s00339-005-3426-7

Frost, G. I., Csoka, T. B., Wong, T., & Stern, R. (1997). Purification, cloning, and expression of human plasma hyaluronidase. *Biochemical and Biophysical Research Communications*, *236*, 10–15. https://doi.org/10.1166/jnn.2007.427

Führmann, T., Obermeyer, J., Tator, C. H., & Shoichet, M. S. (2015). Click-crosslinked injectable hyaluronic acid hydrogel is safe and biocompatible in the intrathecal space for ultimate use in regenerative strategies of the injured spinal cord. *Methods*, *84*, 60–69. https://doi.org/10.1016/j.ymeth.2015.03.023

García-González, C. A., Budtova, T., Durães, L., Erkey, C., Del Gaudio, P., Gurikov, P., Koebel, M., Liebner, F., Neagu, M., & Smirnova, I. (2019). An opinion paper on aerogels for biomedical and environmental applications. *Molecules*, *24*, 1815. https://doi.org/10.3390/molecules24091815

Garcia-Fuentes, M., Giger, E., Meinel, L., & Merkle, H. P. (2008). The effect of hyaluronic acid on silk fibroin conformation. *Biomaterials*, *29*(6), 633–642. https://doi.org/10.1016/j.biomaterials.2007.10.024

Garcia-Fuentes, M., Meinel, A. J., Hilbe, M., Meinel, L., & Merkle, H. P. (2009). Silk fibroin/hyaluronan scaffolds for human mesenchymal stem cell culture in tissue engineering. *Biomaterials*, *30*(28), 5068–5076. https://doi.org/10.1016/j.biomaterials.2009.06.008

González-Nieto, D., Fernández-García, L., Pérez-Rigueiro, J., Guinea, G. V., & Panetsos, F. (2018). Hydrogels-assisted cell engraftment for repairing the stroke-damaged brain: Chimera or reality. *Polymers*, *10*, 184. https://doi.org/10.3390/polym10020184

Haji Mansor, M., Najberg, M., Contini, A., Alvarez-Lorenzo, C., Garcion, E., Jérôme, C., & Boury, F. (2018). Development of a non-toxic and non-denaturing formulation process for encapsulation of SDF-1α into PLGA/PEG-PLGA nanoparticles to achieve sustained release. *European Journal of Pharmaceutics and Biopharmaceutics*, *125*(November 2017), 38–50. https://doi.org/10.1016/j.ejpb.2017.12.020

Haring, A. P., Thompson, E. G., Tong, Y., Laheri, S., Cesewski, E., Sontheimer, H., & Johnson, B. N. (2019). Process- and bio-inspired hydrogels for 3D bioprinting of soft free-standing neural and

glial tissues. *Biofabrication*, *11*(2). https://doi.org/10.1088/1758-5090/ab02c9

Hu, X., Kaplan, D., & Cebe, P. (2006). Determining beta-sheet crystallinity in fibrous proteins by thermal analysis and infrared spectroscopy. *Macromolecules*, *39*(18), 6161–6170. https://doi.org/10.1021/ma0610109

Hu, X., Shmelev, K., Sun, L., Gil, E. S., Park, S. H., Cebe, P., & Kaplan, D. L. (2011). Regulation of silk material structure by temperature-controlled water vapor annealing. *Biomacromolecules*, *12*(5), 1686–1696. https://doi.org/10.1021/bm200062a

Hu, Y., Ran, J., Zheng, Z., Jin, Z., Chen, X., Yin, Z., Tang, C., Chen, Y., Huang, J., Le, H., Yan, R., Zhu, T., Wanga, J., Lin, J., Xu, K., Zhou, Y., Zhang, W., Cai, Y., Dominique, P., Heng, B. C., Chen, W., Shen, W., & Ouyang, H. W. (2018). Exogenous stromal derived factor-1 releasing silk scaffold combined with intra-articular injection of progenitor cells promotes bone-ligament-bone regeneration. *Acta Biomaterialia, 71*, 168–183. https://doi.org/10.1016/j.actbio.2018.02.019

Imitola, J., Raddassi, K., Park, K. I., Mueller, F.-J., Nieto, M., Teng, Y. D., Frenkel, D., Li, J., Sidman, R.L., Walsh, C. A., Snyder, E. Y., Khoury, S. J. (2004). Directed migration of neural stem cells to sites of CNS injury by the stromal cell-derived factor 1 /CXC chemokine receptor 4 pathway. *Proceedings of the National Academy of Sciences*, *101*(52), 18117–18122. https://doi.org/10.1073/pnas.0408258102

Jian, W. H., Wang, H. C., Kuan, C. H., Chen, M. H., Wu, H. C., Sun, J. S., & Wang, T. W. (2018). Glycosaminoglycan-based hybrid hydrogel encapsulated with polyelectrolyte complex nanoparticles for endogenous stem cell regulation in central nervous system regeneration. *Biomaterials*, *174*, 17–30. https://doi.org/10.1016/j.biomaterials.2018.05.009

Jurga, M., Dainiak, M. B., Sarnowska, A., Jablonska, A., Tripathi, A., Plieva, F. M., … McGuckin, C. P. (2011). The performance of laminin-containing cryogel scaffolds in neural tissue regeneration. *Biomaterials*, *32*(13), 3423–3434. https://doi.org/10.1016/j.biomaterials.2011.01.049

Krieger, J. R., Ogle, M. E., McFaline-Figueroa, J., Segar, C. E., Temenoff, J. S., & Botchwey, E. A. (2016). Spatially localized recruitment of anti-inflammatory monocytes by SDF-1α-releasing hydrogels enhances microvascular network remodeling. *Biomaterials*, *77*, 280–290. https://doi.org/10.1016/j.biomaterials.2015.10.045

Kuo, J. W., Swarm, D. A., & Prestwich, G. D. (1991). Chemical modification of hyaluronic acid by carbodiimides. *Bioconjugate Chemistry*, *2*(4), 232–241. https://doi.org/10.1021/bc00010a007

Lassoued, N., Delarue, J., Launay, B., & Michon, C. (2008). Baked product texture: Correlations between instrumental and sensory characterization using Flash Profile. *Journal of Cereal*

561 *Science*, *48*(1), 133–143. https://doi.org/10.1016/j.jcs.2007.08.014

562 Lau, T. T., & Wang, D. A. (2011). Stromal cell-derived factor-1 (SDF-1): Homing factor for engineered
563 regenerative medicine. *Expert Opinion on Biological Therapy*, *11*(2), 189–197.
564 https://doi.org/10.1517/14712598.2011.546338

565 Mahumane, G. D., Kumar, P., Du Toit, L. C., Choonara, Y. E., & Pillay, V. (2018). 3D scaffolds for brain
566 tissue regeneration: Architectural challenges. *Biomaterials Science*, *6*(11), 2812–2837.
567 https://doi.org/10.1039/c8bm00422f

568 Malay, Ö., Bayraktar, O., & Batigün, A. (2007). Complex coacervation of silk fibroin and hyaluronic
569 acid. *International Journal of Biological Macromolecules*, *40*(4), 387–393.
570 https://doi.org/10.1016/j.ijbiomac.2006.09.017

571 Martín-Martín, Y., Fernández-García, L., Sanchez-Rebato, M. H., Marí-Buyé, N., Rojo, F. J., Pérez-
572 Rigueiro, J., Ramos, M., Guinea, G.V., Panetsos, F., & González-Nieto, D. (2019). Evaluation of
573 neurosecretome from mesenchymal stem cells encapsulated in silk fibroin hydrogels. *Scientific*
574 *Reports*, *9*(1), 1–15. https://doi.org/10.1038/s41598-019-45238-4

575 Mazia, D., Schatten, G., & Sale, W. (1975). Adhesion of cells to surfaces coated with polysine.
576 Applications to electron microscopy. *Journal of Cell Biology*, *66*(3), 198–200.

577 Mobini, S., Taghizadeh-Jahed, M., Khanmohammadi, M., Moshiri, A., Naderi, M.-M., Heidari-Vala, H.,
578 Ashrafi Helan, J., Khanjani, S., Springer, A., Akhondi, M. M., & Kazemnejad, S. (2016).
579 Comparative evaluation of *in vivo* biocompatibility and biodegradability of regenerated silk
580 scaffolds reinforced with/without natural silk fibers. *Journal of Biomaterials Applications*, *30*(6),
581 793–809. https://doi.org/10.1177/0885328215601925

582 Modo, M. (2019). Bioscaffold-induced brain tissue regeneration. *Frontiers in Neuroscience, 13*, 1156.
583 https://doi.org/10.3389/fnins.2019.01156

584 Monneau, Y., Arenzana-Seisdedos, F., & Lortat-Jacob, H. (2016). The sweet spot: how GAGs help
585 chemokines guide migrating cells. *Journal of Leukocyte Biology*, *99*(6), 935–953.
586 https://doi.org/10.1189/jlb.3mr0915-440r

587 Murphy, M. C., Huston, J., Jack, C. R., Glaser, K. J., Manduca, A., Felmlee, J. P., & Ehman, R. L. (2011).
588 Decreased brain stiffness in Alzheimer's disease determined by magnetic resonance
589 elastography. *Journal of Magnetic Resonance Imaging*, *34*(3), 494–498.
590 https://doi.org/10.1002/jmri.22707

591 Najberg, M., Haji Mansor, M., Boury, F., Alvarez-Lorenzo, C., & Garcion, E. (2019). Reversing the
592 tumor target: establishment of a tumor trap. *Frontiers in Pharmacology*, *10*(August), 1–12.

https://doi.org/10.3389/fphar.2019.00887

Nava, M. M., Raimondi, M. T., & Pietrabissa, R. (2012). Controlling self-renewal and differentiation of stem cells via mechanical cues. *Journal of Biomedicine and Biotechnology*, *2012*, 1–12. https://doi.org/10.1155/2012/797410

Nicholson, C., & Syková, E. (1998). Extracellular space structure revealed by diffusion analysis. *Trends in Neurosciences*, *21*, 207–215. https://doi.org/10.1016/S0166-2236(98)01261-2

Nultsch, K., & Germershaus, O. (2017). Silk fibroin degumming affects scaffold structure and release of macromolecular drugs. *European Journal of Pharmaceutical Sciences*, *106*(June), 254–261. https://doi.org/10.1016/j.ejps.2017.06.012

Orive, G., Anitua, E., Pedraz, J. L., & Emerich, D. F. (2009). Biomaterials for promoting brain protection, repair and regeneration. *Nature Reviews Neuroscience*, *10*(9), 682–692. https://doi.org/10.1038/nrn2685

Park, S.H., Gil, E.S., Shi, H., Kim, H.J., Lee, K., Kaplan, D.L. (2010). Relationships between degradability of silk scaffolds and osteogenesis. *Biomaterials, 31*(24), 6162-6172. https://doi.org/10.1016/j.biomaterials.2010.04.028

Prokoph, S., Chavakis, E., Levental, K. R., Zieris, A., Freudenberg, U., Dimmeler, S., & Werner, C. (2012). Sustained delivery of SDF-1alpha from heparin-based hydrogels to attract circulating pro-angiogenic cells. *Biomaterials*, *33*(19), 4792–4800. https://doi.org/10.1016/j.biomaterials.2012.03.039

Purcell, B. P., Elser, J. A., Mu, A., Margulies, K. B., & Burdick, J. A. (2012). Synergistic effects of SDF-1α chemokine and hyaluronic acid release from degradable hydrogels on directing bone marrow derived cell homing to the myocardium. *Biomaterials*, *33*(31), 7849–7857. https://doi.org/10.1016/j.biomaterials.2012.07.005

Rabbany, S. Y., Pastore, J., Yamamoto, M., Miller, T., Rafii, S., Aras, R., & Penn, M. (2010). Continuous delivery of stromal cell-derived factor-1 from alginate scaffolds accelerates wound healing. *Cell Transplantation*, *19*(4), 399–408. https://doi.org/10.3727/096368909X481782

Rockwood, D. N., Preda, R. C., Yücel, T., Wang, X., Lovett, M. L., & Kaplan, D. L. (2011). Materials fabrication from *Bombyx mori* silk fibroin. *Nature Protocols*, *6*(10), 1612–1631. https://doi.org/10.1038/nprot.2011.379

Rouslahti, E. (1996). Brain extracellular matrix. *Glycobiology*, *6*(5), 489–492.

Sadir, R., Baleux, F., Grosdidier, A., Imberty, A., & Lortat-Jacob, H. (2001). Characterization of the

stromal cell-derived factor-1alpha-heparin complex. *J Biol Chem*, *276*(11), 8288–8296. https://doi.org/10.1074/jbc.M008110200

Seyedhassantehrani, N., Li, Y., & Yao, L. (2016). Dynamic behaviors of astrocytes in chemically modified fibrin and collagen hydrogels. *Integrative Biology (United Kingdom)*, *8*(5), 624–634. https://doi.org/10.1039/c6ib00003g

Thurber, A. E., Omenetto, F. G., & Kaplan, D. L. (2015). In vivo bioresponses to silk proteins. *Biomaterials*, *71*(2015), 145–157. https://doi.org/10.1016/j.biomaterials.2015.08.039

Vepari, C., & Kaplan, D. L. (2012). Silk as biomaterial. *Progress in Polymer Science*, *100*(2), 130–134. https://doi.org/10.1016/j.pestbp.2011.02.012.

Wang, C., Tong, X., & Yang, F. (2014). Bioengineered 3D Brain tumor model to elucidate the effects of matrix stiffness on glioblastoma cell behavior using peg-based hydrogels. *Molecular Pharmaceutics*, *11*, 2115–2125. https://doi.org/dx.doi.org/10.1021/mp5000828 |

Weickenmeier, J., de Rooij, R., Budday, S., Steinmann, P., Ovaert, T. C., & Kuhl, E. (2016). Brain stiffness increases with myelin content. *Acta Biomaterialia*, *42*, 265–272. https://doi.org/10.1016/j.actbio.2016.07.040

Wentao, Z., Ya'nan, H., Jian, L., Kaipeng, B., Peng, S., Yu, Z., Peng, Z., Huanxiang, Z., Feng, Z., & Yixin, S. (2019). *In vitro* biocompatibility study of a water-rinsed biomimetic silk porous scaffold with olfactory ensheathing cells. *International Journal of Biological Macromolecules*, *125*, 526–533. https://doi.org/10.1016/j.ijbiomac.2018.11.029

Xia, M., Huang, R., Witt, K. L., Southall, N., Fostel, J., Cho, M. H., Jadhav, A., Smith, C. S., Inglese, J., Portier, C. J., Tice, R. R., & Austin, C. P. (2008). Compound cytotoxicity profiling using quantitative high-throughput screening. *Environmental Health Perspectives*, *116*(3), 284–291. https://doi.org/10.1289/ehp.10727

Yamada, H., Nakao, H., Takasu, Y., & Tsubouchi, K. (2001). Preparation of undegraded native molecular fibroin solution from silkworm cocoons. *Materials Science and Engineering: C*, *14*(1), 41–46. https://doi.org/10.1016/S0928-4931(01)00207-7

Yang, J. W., Zhang, Y. F., Wan, C. Y., Sun, Z. Y., Nie, S., Jian, S. J., Zhang, L., Song, G. T., & Chen, Z. (2015). Autophagy in SDF-1a-mediated DPSC migration and pulp regeneration. *Biomaterials*, *44*, 11–23. https://doi.org/10.1016/j.biomaterials.2014.12.006

Zhao, W., Jin, K., Li, J., Qiu, X., & Li, S. (2017). Delivery of stromal cell-derived factor 1α for *in situ* tissue regeneration. *Journal of Biological Engineering*, *11*(1), 1–12. https://doi.org/10.1186/s13036-017-0058-3